CLNS 99/1650
CLEO 99-18

Study of Two-Body B Decays to Kaons and Pions: Observation of $B \to \pi^+\pi^-$, $B \to K^\pm\pi^0$, and $B \to K^0\pi^0$ Decays.

(CLEO Collaboration)

(February 7, 2008)

Abstract

We have studied charmless hadronic decays of B mesons into two-body final states with kaons and pions and observe three new processes with the following branching fractions: $\mathcal{B}(B \to \pi^+\pi^-) = (4.3^{+1.6}_{-1.4} \pm 0.5) \times 10^{-6}$, $\mathcal{B}(B \to K^0\pi^0) = (14.6^{+5.9+2.4}_{-5.1-3.3}) \times 10^{-6}$, and $\mathcal{B}(B \to K^\pm\pi^0) = (11.6^{+3.0+1.4}_{-2.7-1.3}) \times 10^{-6}$. We also update our previous measurements for the decays $B \to K^\pm\pi^\mp$ and $B^\pm \to K^0\pi^\pm$.

D. Cronin-Hennessy,[1] Y. Kwon,[1,*] A.L. Lyon,[1] E. H. Thorndike,[1] C. P. Jessop,[2] H. Marsiske,[2] M. L. Perl,[2] V. Savinov,[2] D. Ugolini,[2] X. Zhou,[2] T. E. Coan,[3] V. Fadeyev,[3] Y. Maravin,[3] I. Narsky,[3] R. Stroynowski,[3] J. Ye,[3] T. Wlodek,[3] M. Artuso,[4] R. Ayad,[4] C. Boulahouache,[4] K. Bukin,[4] E. Dambasuren,[4] S. Karamnov,[4] S. Kopp,[4] G. Majumder,[4] G. C. Moneti,[4] R. Mountain,[4] S. Schuh,[4] T. Skwarnicki,[4] S. Stone,[4] G. Viehhauser,[4] J.C. Wang,[4] A. Wolf,[4] J. Wu,[4] S. E. Csorna,[5] I. Danko,[5] K. W. McLean,[5] Sz. Márka,[5] Z. Xu,[5] R. Godang,[6] K. Kinoshita,[6,†] I. C. Lai,[6] S. Schrenk,[6] G. Bonvicini,[7] D. Cinabro,[7] L. P. Perera,[7] G. J. Zhou,[7] G. Eigen,[8] E. Lipeles,[8] M. Schmidtler,[8] A. Shapiro,[8] W. M. Sun,[8] A. J. Weinstein,[8] F. Würthwein,[8,‡] D. E. Jaffe,[9] G. Masek,[9] H. P. Paar,[9] E. M. Potter,[9] S. Prell,[9] V. Sharma,[9] D. M. Asner,[10] A. Eppich,[10] J. Gronberg,[10] T. S. Hill,[10] D. J. Lange,[10] R. J. Morrison,[10] H. N. Nelson,[10] R. A. Briere,[11] B. H. Behrens,[12] W. T. Ford,[12] A. Gritsan,[12] J. Roy,[12] J. G. Smith,[12] J. P. Alexander,[13] R. Baker,[13] C. Bebek,[13] B. E. Berger,[13] K. Berkelman,[13] F. Blanc,[13] V. Boisvert,[13] D. G. Cassel,[13] M. Dickson,[13] P. S. Drell,[13] K. M. Ecklund,[13] R. Ehrlich,[13] A. D. Foland,[13] P. Gaidarev,[13] L. Gibbons,[13] B. Gittelman,[13] S. W. Gray,[13] D. L. Hartill,[13] B. K. Heltsley,[13] P. I. Hopman,[13] C. D. Jones,[13] D. L. Kreinick,[13] M. Lohner,[13] A. Magerkurth,[13] T. O. Meyer,[13] N. B. Mistry,[13] C. R. Ng,[13] E. Nordberg,[13] J. R. Patterson,[13] D. Peterson,[13] D. Riley,[13] J. G. Thayer,[13] P. G. Thies,[13] B. Valant-Spaight,[13] A. Warburton,[13] P. Avery,[14] C. Prescott,[14] A. I. Rubiera,[14] J. Yelton,[14] J. Zheng,[14] G. Brandenburg,[15] A. Ershov,[15] Y. S. Gao,[15] D. Y.-J. Kim,[15] R. Wilson,[15] T. E. Browder,[16] Y. Li,[16] J. L. Rodriguez,[16] H. Yamamoto,[16] T. Bergfeld,[17] B. I. Eisenstein,[17] J. Ernst,[17] G. E. Gladding,[17] G. D. Gollin,[17] R. M. Hans,[17] E. Johnson,[17] I. Karliner,[17] M. A. Marsh,[17] M. Palmer,[17] C. Plager,[17] C. Sedlack,[17] M. Selen,[17] J. J. Thaler,[17] J. Williams,[17] K. W. Edwards,[18] R. Janicek,[19] P. M. Patel,[19] A. J. Sadoff,[20] R. Ammar,[21] A. Bean,[21] D. Besson,[21] R. Davis,[21] I. Kravchenko,[21] N. Kwak,[21] X. Zhao,[21] S. Anderson,[22] V. V. Frolov,[22] Y. Kubota,[22] S. J. Lee,[22] R. Mahapatra,[22] J. J. O'Neill,[22] R. Poling,[22] T. Riehle,[22] A. Smith,[22] J. Urheim,[22] S. Ahmed,[23] M. S. Alam,[23] S. B. Athar,[23] L. Jian,[23] L. Ling,[23] A. H. Mahmood,[23,§] M. Saleem,[23] S. Timm,[23] F. Wappler,[23] A. Anastassov,[24] J. E. Duboscq,[24] K. K. Gan,[24] C. Gwon,[24] T. Hart,[24] K. Honscheid,[24] D. Hufnagel,[24] H. Kagan,[24] R. Kass,[24] J. Lorenc,[24] T. K. Pedlar,[24] H. Schwarthoff,[24] E. von Toerne,[24] M. M. Zoeller,[24] S. J. Richichi,[25] H. Severini,[25] P. Skubic,[25] A. Undrus,[25] S. Chen,[26] J. Fast,[26] J. W. Hinson,[26] J. Lee,[26] N. Menon,[26] D. H. Miller,[26] E. I. Shibata,[26] I. P. J. Shipsey,[26] and V. Pavlunin[26]

[1]University of Rochester, Rochester, New York 14627
[2]Stanford Linear Accelerator Center, Stanford University, Stanford, California 94309
[3]Southern Methodist University, Dallas, Texas 75275

*Permanent address: Yonsei University, Seoul 120-749, Korea.

†Permanent address: University of Cincinnati, Cincinnati OH 45221

‡Permanent address: Massachusetts Institute of Technology, Cambridge, MA 02139.

§Permanent address: University of Texas - Pan American, Edinburg TX 78539.

[4]Syracuse University, Syracuse, New York 13244
[5]Vanderbilt University, Nashville, Tennessee 37235
[6]Virginia Polytechnic Institute and State University, Blacksburg, Virginia 24061
[7]Wayne State University, Detroit, Michigan 48202
[8]California Institute of Technology, Pasadena, California 91125
[9]University of California, San Diego, La Jolla, California 92093
[10]University of California, Santa Barbara, California 93106
[11]Carnegie Mellon University, Pittsburgh, Pennsylvania 15213
[12]University of Colorado, Boulder, Colorado 80309-0390
[13]Cornell University, Ithaca, New York 14853
[14]University of Florida, Gainesville, Florida 32611
[15]Harvard University, Cambridge, Massachusetts 02138
[16]University of Hawaii at Manoa, Honolulu, Hawaii 96822
[17]University of Illinois, Urbana-Champaign, Illinois 61801
[18]Carleton University, Ottawa, Ontario, Canada K1S 5B6
and the Institute of Particle Physics, Canada
[19]McGill University, Montréal, Québec, Canada H3A 2T8
and the Institute of Particle Physics, Canada
[20]Ithaca College, Ithaca, New York 14850
[21]University of Kansas, Lawrence, Kansas 66045
[22]University of Minnesota, Minneapolis, Minnesota 55455
[23]State University of New York at Albany, Albany, New York 12222
[24]Ohio State University, Columbus, Ohio 43210
[25]University of Oklahoma, Norman, Oklahoma 73019
[26]Purdue University, West Lafayette, Indiana 47907

CP violation in the Standard Model (SM) arises naturally from the complex phase in the Cabibbo-Kobayashi-Maskawa (CKM) quark-mixing matrix [1]. This picture is supported by numerous experimental constraints [2], as well as recent observation of direct CP violation in the kaon system [3], but it remains an open experimental question whether this phase is the only source of CP violation in nature. Studies of the rare charmless decays of B mesons are likely to play an important role in constraining the CKM matrix and testing the SM picture of CP violation.

Several approaches have been suggested to extract this phase information from measurements of rare B decays. Ratios of various $B \to K\pi$ branching fractions were shown [4] to depend explicitly on $\gamma \equiv Arg(V_{ub}^*)$ with relatively modest model dependence. Within a factorization model, branching fractions of a large number of rare B decays can be parametrized by a small number of independent physical quantities, including γ, which can then be extracted through a global fit [5] to existing data. Finally, measurement of the time-dependent CP-violating asymmetry in the decay $B^0 \to \pi^+\pi^-$ can be used to determine the sum of γ and the phase $\beta \equiv Arg(V_{td}^*)$. In this case additional measurements of other isospin-related $B \to \pi\pi$ processes are required to allow extraction of $\gamma + \beta$ [6].

In this Letter we present new measurements of $B \to K\pi$ and $B \to \pi\pi$ branching fractions with significantly increased statistics, superseding results from our previous publication [7]. In particular we present first observations of the long-awaited mode $B \to \pi^+\pi^-$, as well as $B \to K^\pm\pi^0$ and $B \to K^0\pi^0$ decays.

The data used in this analysis were collected with the CLEO II detector at the Cornell Electron Storage Ring (CESR). It consists of 9.13 fb^{-1} taken at the Υ(4S), corresponding to 9.66M $B\bar{B}$ pairs, and 4.35 fb^{-1} taken below $B\bar{B}$ threshold, used for continuum background studies.

CLEO II is a general purpose solenoidal magnet detector, described in detail elsewhere [8]. Cylindrical drift chambers in a 1.5T solenoidal magnetic field measure momentum and specific ionization (dE/dx) of charged particles. Photons are detected using a 7800-crystal CsI(Tl) electromagnetic calorimeter. In the CLEO II.V detector configuration, the innermost chamber was replaced by a 3-layer, double-sided silicon vertex detector, and the gas in the main drift chamber was changed from an argon-ethane to a helium-propane mixture. As a result of these modifications, the CLEO II.V portion of the data (2/3 of the total) has significantly improved particle identification and momentum resolution.

Efficient track quality requirements are imposed on charged tracks, and pions and kaons are identified by dE/dx. The separation between kaons and pions for typical signal momenta $p \sim 2.6$ GeV/c is 1.7 standard deviations (σ) for CLEO II data and 2.0 σ for CLEO II.V data. Candidate K_S^0 are selected from pairs of tracks forming well-measured displaced vertices with a $\pi^+\pi^-$ invariant mass within 2σ of the nominal K_S^0 mass. Pairs of photons with an invariant mass within 2.5σ of the nominal π^0 mass are kinematically fitted with the mass constrained to the nominal π^0 mass. Electrons are rejected based on dE/dx and the ratio of the track momentum to the associated shower energy in the CsI calorimeter; muons are rejected based on the penetration depth in the instrumented steel flux return.

The B decay candidate is identified via invariant mass and total energy of its decay products. We calculate a beam-constrained B mass $M = \sqrt{E_{\rm b}^2 - p_B^2}$, where p_B is the B candidate momentum and $E_{\rm b}$ is the beam energy. The resolution in M is dominated by the beam energy spread and ranges from 2.5 to 3.0 MeV, where the larger resolution corresponds to decay modes with a π^0. We define $\Delta E = E_1 + E_2 - E_{\rm b}$, where E_1 and E_2 are the energies of the daughters of the B meson candidate. The resolution in ΔE is mode-dependent. For final states without π^0's, the ΔE

resolution is 20 MeV (25 MeV in CLEO II). For modes with π^0's the ΔE resolution is worse by approximately a factor of two and becomes slightly asymmetric because of energy loss out of the back of the CsI crystals. We accept events with M within $5.2-5.3$ GeV and $|\Delta E| < 200$ MeV. This fiducial region includes the signal region and a generous sideband for background normalization. $\pi\pi$ and $K\pi$ signal events are distinguished both by dE/dx and ΔE observables. The ΔE distribution for $B \to K^+\pi^-$, calculated under the replacement of m_K by m_π, is centered at -42 MeV, giving a separation of 2.1σ(1.7σ in CLEO II) between $B \to K^+\pi^-$ and $B \to \pi^+\pi^-$.

We have studied backgrounds from $b \to c$ decays and other $b \to u$ and $b \to s$ decays and find that all are negligible for the analyses presented here. The main background arises from $e^+e^- \to q\bar{q}$ (where $q = u, d, s, c$). Such events typically exhibit a two-jet structure and can produce high momentum back-to-back tracks in the fiducial region. To reduce contamination from these events, we calculate the angle θ_S between the sphericity axis [9] of the candidate tracks and showers and the sphericity axis of the rest of the event. The distribution of $\cos\theta_S$ is strongly peaked at ± 1 for $q\bar{q}$ events and is nearly flat for $B\bar{B}$ events. We require $|\cos\theta_S| < 0.8$ which eliminates 83% of the background. Using a detailed GEANT-based Monte Carlo simulation [10] we determine overall detection efficiencies $\mathcal{E}$ of $11-48\%$, as listed in Table I. Efficiencies include the branching fractions for $K^0 \to K^0_S \to \pi^+\pi^-$ and $\pi^0 \to \gamma\gamma$ where applicable.

Additional discrimination between isotropic signal and rather jetty $q\bar{q}$ background is provided by the cosine of the angle between the candidate sphericity axis and beam axis (expected to be isotropic for signal, $1 + cos^2\theta$ distribution for $q\bar{q}$ background); the ratio of Fox-Wolfram moments H_2/H_0 [11] (expected to be smaller for signal than for background); and the distribution of the energy from the rest of the event relative to the candidate's sphericity axis, as characterized by the energy in nine 10° angular bins. These 11 variables are combined by a Fisher discriminant technique as described in detail in Ref. [12] The Fisher discriminant is a linear combination of experimental observables $\mathcal{F} \equiv \sum_{i=1}^{N} \alpha_i y_i$, where the coefficients α_i are chosen to maximize the separation between the simulated signal and background samples.

We perform unbinned maximum-likelihood fits using ΔE, M, $\mathcal{F}$, the angle between the B meson momentum and beam axis, and dE/dx (where applicable) as input information for each candidate event to determine the signal yields. Four different fits are performed, one for each topology (h^+h^-, $h^\pm\pi^0$, $h^\pm K^0_S$, and $K^0_S\pi^0$, $h^\pm$ referring to a charged kaon or pion). In each of these fits, the likelihood of the event is parametrized by the sum of probabilities for all relevant signal and background hypotheses, with relative weights determined by maximizing the likelihood function $\mathcal{L}$. The probability of a particular hypothesis is calculated as a product of the probability density functions (PDFs) for each of the input variables. Further details about the likelihood fit can be found in Ref. [12]. The parameters for the PDFs are determined from independent data and high-statistics Monte Carlo samples. We estimate a systematic error on the fitted yield by varying the PDFs used in the fit within their uncertainties. These uncertainties are dominated by the limited statistics in the independent data samples we used to determine the PDFs. The systematic errors on the measured branching fractions are obtained by adding this fit systematic in quadrature with the systematic error on the efficiency.

Figure 1a shows the results of the likelihood fit for $B \to \pi^+\pi^-$ and $B \to K^\pm\pi^\mp$. The curves represent the $n\sigma$ contours, which correspond to the increase in $-2\ln\mathcal{L}$ by n^2. Systematic uncertainties are not included in any contour plots. The statistical significance of a given signal yield is determined by repeating the fit with the signal yield fixed to be zero and recording the change in $-2\ln\mathcal{L}$. We also compute from the PDFs the event-by-event probability to be signal or continuum

TABLE I. Summary of experimental results. The errors on branching fractions $\mathcal{B}$ are statistical and systematic respectively. Reconstruction efficiency $\mathcal{E}$ includes branching fractions of $K^0 \to K^0_S \to \pi^+\pi^-$ and $\pi^0 \to \gamma\gamma$ when applicable. We assume equal branching fraction for $\Upsilon(4s) \to B^0\bar{B}^0$ and B^+B^-. Theoretical predictions are taken from Ref. 13.

Mode	N_S	Sig.	$\mathcal{E}(\%)$	$\mathcal{B} \times 10^6$	Theory $\mathcal{B} \times 10^6$
$\pi^+\pi^-$	$20.0^{+7.6}_{-6.5}$	4.2σ	48	$4.3^{+1.6}_{-1.4} \pm 0.5$	8–26
$\pi^\pm\pi^0$	$21.3^{+9.7}_{-8.5}$	3.2σ	39	< 12.7	3–20
$K^\pm\pi^\mp$	$80.2^{+11.8}_{-11.0}$	11.7σ	48	$17.2^{+2.5}_{-2.4} \pm 1.2$	7–24
$K^\pm\pi^0$	$42.1^{+10.9}_{-9.9}$	6.1σ	38	$11.6^{+3.0+1.4}_{-2.7-1.3}$	3–15
$K^0\pi^\pm$	$25.2^{+6.4}_{-5.6}$	7.6σ	14	$18.2^{+4.6}_{-4.0} \pm 1.6$	8–26
$K^0\pi^0$	$16.1^{+5.9}_{-5.0}$	4.9σ	11	$14.6^{+5.9+2.4}_{-5.1-3.3}$	3–9
K^+K^-	$0.7^{+3.4}_{-0.7}$	0.0σ	48	< 1.9	–
$K^\pm\bar{K}^0$	$1.4^{+2.4}_{-1.3}$	1.1σ	14	< 5.1	0.7–1.5

background, as well as the probability to be $K\pi$-like or $\pi\pi$-like. From these we form likelihood ratios, $\mathcal{R}_{sig} = (P^s_{\pi\pi} + P^s_{K\pi})/(P^s_{\pi\pi} + P^s_{K\pi} + P^c_{\pi\pi} + P^c_{K\pi} + P^c_{KK})$ and $\mathcal{R}_\pi = P^s_{\pi\pi}/(P^s_{\pi\pi} + P^s_{K\pi})$. Superscripts s and c denote signal and continuum background respectively. Figure 1b illustrates the distribution of events in $\mathcal{R}_{sig}$ (vertical axis) and $\mathcal{R}_\pi$ (horizontal axis). The cluster of events in the upper right corner is clear evidence for $B \to \pi^+\pi^-$.

Figures 1(c-f) show distributions in M and ΔE for events after cuts on likelihood ratios $\mathcal{R}_{sig}$ and $\mathcal{R}_\pi$ computed without M and ΔE, respectively. The likelihood fit projections for signal and background components, suitably scaled to account for the efficiencies of the additional cuts (50-70 % for signal), are overlaid. Figure 2 shows the likelihood functions for the fits to $B \to K^0\pi^0$ and $B \to h^\pm\pi^0$. Figure 3 shows M and ΔE distributions for $B \to K^0\pi^\pm$, $B \to K^\pm\pi^0$, and $B \to K^0\pi^0$.

We summarize all branching fractions and upper limits in Table I. In addition to the first observations $B \to \pi^+\pi^-$, $B \to K^+\pi^0$, and $B \to K^0\pi^0$, we report improved measurements for the decays $B \to K^\pm\pi^\mp$ and $B \to K^0\pi^\pm$. The table also includes a range of theoretical predictions taken from recent literature [13]. We see some indication for the decay $B \to \pi^\pm\pi^0$ with the branching fraction of $\mathcal{B}(B \to \pi^\pm\pi^0) = (5.6^{+2.6}_{-2.3} \pm 1.7) \times 10^{-6}$, but statistical significance of the signal yield is insufficient to claim an observation for this decay mode. We find no evidence for the decays $B \to K^+K^-$ and $B \to K^\pm K^0$, and calculate 90% confidence level (CL) upper limit yields by integrating the likelihood function

$$\frac{\int_0^{N^{UL}} \mathcal{L}_{\max}(N)dN}{\int_0^{\infty} \mathcal{L}_{\max}(N)dN} = 0.90 \qquad (1)$$

where $\mathcal{L}_{\max}(N)$ is the maximum $\mathcal{L}$ at fixed N to conservatively account for possible correlations among the free parameters in the fit. We then increase upper limit yields by their systematic errors and reduce detection efficiencies by their systematic errors to calculate branching fraction upper limits given in Table I.

To evaluate how systematic uncertainties in the PDFs affect the statistical significance for modes where we report first observations, we repeated the fits for the h^+h^-, $h^+\pi^0$ and $K^0\pi^0$ modes with all PDFs changed simultaneously within their uncertainties to maximally reduce the

signal yield in the modes of interest. Under these extreme conditions, the significance of the first-observation modes $\pi^+\pi^-$, $K^+\pi^0$ and $K^0\pi^0$ becomes 3.2, 5.3 and 3.8 σ respectively. We also evaluate the branching fractions with alternative analyses using tighter and looser cuts on the continuum-suppressing variable $|\cos\theta_S|$. These variations correspond to halving and doubling the background in the fitted sample. The changes in branching fractions under these variations are insignificant compared to the statistical error of our results.

The ratio of the branching fractions $\mathcal{B}(B \to K^\pm K^0)/\mathcal{B}(B \to \pi^\pm K^0)$ can be used to estimate the size of final state interactions in charmless rare B decays [14]. Following the method outlined above we calculate $\mathcal{B}(B \to K^\pm K^0)/\mathcal{B}(B \to \pi^\pm K^0) < 0.3$ at 90% CL. It has also been suggested [15] to use the ratio of the branching fractions $\mathcal{B}(B \to K^\pm\pi^\mp)/\mathcal{B}(B \to \pi^+\pi^-)$ to estimate uncertainties in the measurement of the unitarity triangle parameter $\alpha = \pi - \beta - \gamma$ via $B^0(t) \to \pi^+\pi^-$. We obtain $\mathcal{B}(B \to K^\pm\pi^\mp)/\mathcal{B}(B \to \pi^+\pi^-) < 15$ at 90% CL which implies that an error on α obtained from time-dependent asymmetry measurements of $B^0 \to \pi^+\pi^-$ can be as high as 60° [15].

In summary: we have made a first observation of $B \to \pi^+\pi^-$; measured branching fractions for all four exclusive $B \to K\pi$, including first observations of the decays $B \to K^+\pi^0$ and $B \to K^0\pi^0$; obtained improved upper limits on $B \to \pi^+\pi^0$ and $B \to K\bar{K}$ modes. The hierarchy of branching fractions $KK < \pi\pi < K\pi$ is obvious.

We thank W.-S. Hou for many useful discussions. We gratefully acknowledge the effort of the CESR staff in providing us with excellent luminosity and running conditions. This work was supported by the National Science Foundation, the U.S. Department of Energy, the Research Corporation, the Natural Sciences and Engineering Research Council of Canada, the A.P. Sloan Foundation, the Swiss National Science Foundation, and Alexander von Humboldt Stiftung.

REFERENCES

[1] M. Kobayashi and K. Maskawa, Prog. Theor. Phys. **49**, 652 (1973).

[2] A.J. Buras, Lectures given at the 14th Lake Louise Winter Institute, February 1999, hep-ph/9905437.

[3] A. Alavi-Harati *et al.* (KTeV), Phys. Rev. Lett. **83**, 22 (1999); V. Fanti *et al.* (NA48). Phys. Lett. B **465**, 335 (1999).

[4] M. Gronau, J. L. Rosner, and D. London, Phys. Rev. Lett. **73**, 21 (1994); R. Fleischer, Phys. Lett. B **365**, 399 (1996); R. Fleischer and T. Mannel, Phys. Rev. D **57**, 2752 (1998). M. Neubert and J. Rosner, Phys. Lett. B **441**, 403 (1998); M. Neubert, J. High Energy Phys. **02** (1999) 014.

[5] W.-S. Hou, J. G. Smith, and F. Würthwein, hep-ex/9910014.

[6] M. Gronau and D. London, Phys. Rev. Lett. **65**, 3381 (1990).

[7] R. Godang *et al.* (CLEO Collaboration), Phys. Rev. Lett. **80**, 3456 (1998).

[8] Y. Kubota *et al.* (CLEO Collaboration), Nucl. Instrum. Methods Phys. Res., Sec. A**320**, 66 (1992); T.S. Hill, Nucl. Instrum. Methods Phys. Res., Sec. A **418**, 32 (1998).

[9] S. L. Wu, Phys. Rep. C**107**, 59 (1984).

[10] R. Brun *et al.*, GEANT 3.15, CERN DD/EE/84-1.

[11] G. Fox and S. Wolfram, Phys. Rev. Lett. **41**, 1581 (1978).

[12] D. M. Asner *et al.* (CLEO Collaboration), Phys. Rev. D **53**, 1039 (1996).

[13] N. G. Deshpande and J. Trampetic, Phys. Rev. D **41**, 895 (1990); L.-L. Chau *et al.*, Phys. Rev. D **43**, 2176 (1991); A. Deandrea *et al.*, Phys. Lett. B **318**, 549 (1993); A. Deandrea *et al.*, Phys. Lett. B **320**, 170 (1994); G. Kramer, W. F. Palmer, and H. Simma, Z. Phys. C **66**, 429 (1995); G. Kramer and W. F. Palmer, Phys. Rev. D **52**, 6411 (1995); D. Ebert, R. N. Faustov, and V. O. Galkin, Phys. Rev. D **56**, 312 (1997); D. Du and L. Guo, Zeit. Phys. C **75**, 9 (1997); N.G. Deshpande, B. Dutta, and S. Oh, Phys. Rev. D **57**, 5723 (1998); H. Cheng and B. Tseng, Phys. Rev. D **58**, (1998) 094005; A. Ali, G. Kramer, and C. Lü, Phys. Rev. D **58**, (1998) 094009.

[14] A. F. Falk, A. L. Kagan, Y. Nir, and A. A. Petrov, Phys. Rev. D **57**, 4290 (1998).

[15] J. Charles, Phys. Rev. D **59**, 054007 (1999).

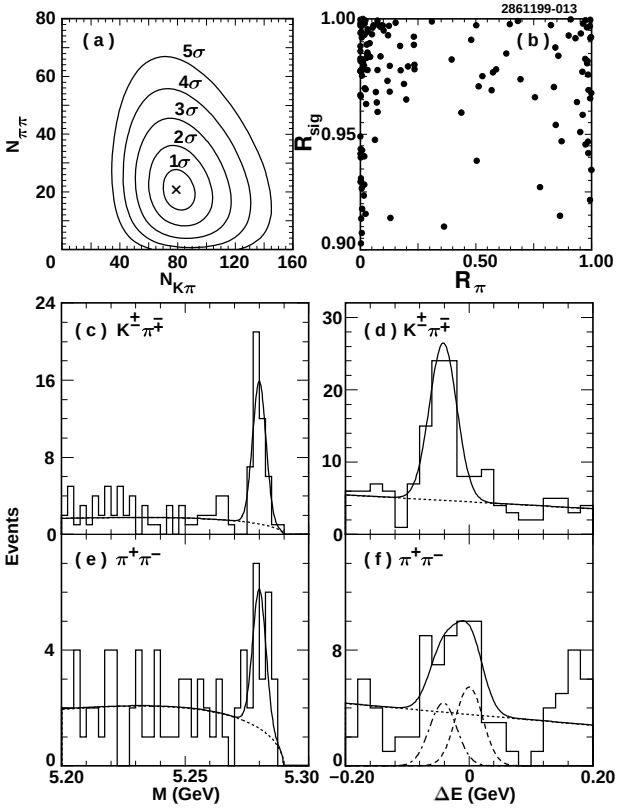

FIG. 1. Results for $B \to K^\pm\pi^\mp$ and $B \to \pi^+\pi^-$. Contours of the likelihood function versus $K\pi$ and $\pi\pi$ event yield (a); likelihood ratios (b) − signal events cluster near the top of the figure, and separate into $K\pi$-like events on the left and $\pi\pi$-like events on the right; beam constrained mass for $K\pi$-like events (c); ΔE for $K\pi$-like events (d); beam constrained mass for $\pi\pi$-like events (e); ΔE for $\pi\pi$-like events (f), with both $\pi\pi$ signal (dashed line) and $K\pi$ cross-feed (dot-dashed line) shown.

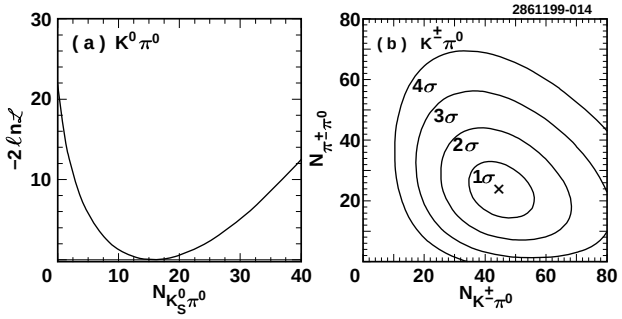

FIG. 2. Likelihood function versus event yield for $B \to K^0\pi^0$ (a) and likelihood contours for $B \to h^\pm\pi^0$ (b).

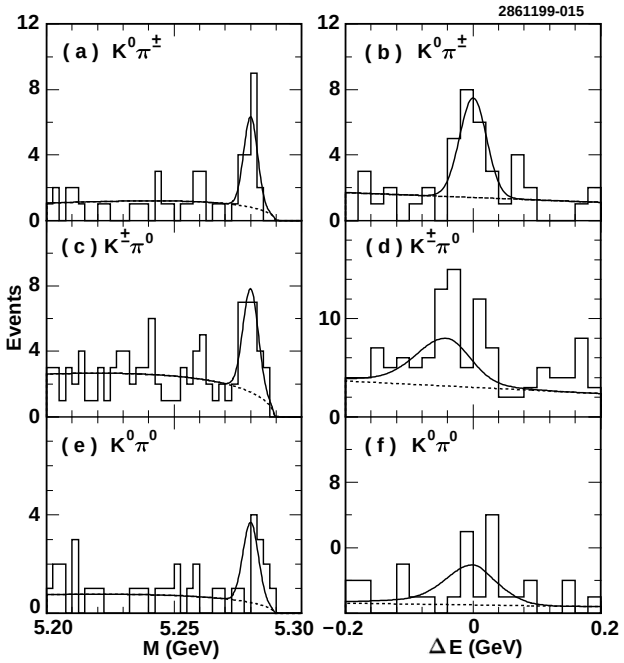

FIG. 3. Beam constrained mass and ΔE distributions for $B \to K^0\pi^\pm$ (a-b), $B \to K^\pm\pi^0$ (c-d), and $B \to K^0\pi^0$ (e-f).